OFFPRINT

Huge broadening of the crystal-fluid interface for sedimenting colloids

E. ALLAHYAROV and H. LÖWEN

Please visit the new website
www.epljournal.org

Huge broadening of the crystal-fluid interface for sedimenting colloids

E. Allahyarov[1,2,3](a) and H. Löwen[1]

[1] *Institut für Theoretische Physik, Heinrich-Heine-Universität Düsseldorf - D-40225 Düsseldorf, Germany*
[2] *Joint Institute for High Temperatures, Russian Academy of Sciences - Izhorskaya 13/19, 117419 Moscow, Russia*
[3] *Department of Physics, Case Western Reserve University - Cleveland, 44106 OH, USA*

Abstract – For sedimenting colloidal hard spheres, the propagation and broadening of the crystal-fluid interface is studied by Brownian dynamics computer simulations of an initially homogeneous sample. Two different types of interface broadenings are observed: the first occurs during growth and is correlated with the interface velocity, the second is concomitant with the splitting of the crystal-fluid interface into the crystal-amorphous and amorphous-liquid interfaces. The latter width is strongly peaked as a function of the gravitational driving strength with a huge amplitude relative to its equilibrium counterpart.

Introduction. – Sedimentation of colloidal particles in a liquid is a widespread phenomenon which governs the formation of river sediments close to salty sea water [1], controls the function of red blood cells [2], and is technologically used to separate different sorts of particles by centrifugation [3]. Gravity is also used to compactify colloidal samples. In a finite container, the actual settling process reaches a sedimentation-diffusion equilibrium, which is characterized by a static colloidal density profile. Much of our particle-resolved knowledge of dense suspensions stems from model hard-sphere colloidal dispersions made up of sterically stabilized particles. In equilibrium, it has been shown that density profiles contain the isothermal equation of state of the hard-sphere system [4,5]. At high gravitational strengths (or Péclet numbers) the density of hard spheres at the bottom of suspension increases above the lower limit of the solid-liquid coexistence $\phi = 0.492$ [6], and a crystallization in the bottom layers occurs [7–9]. The number of crystalline layers is controlled by gravity and by the sedimentation velocity of particles, and the overall particle density per area. While the equilibrium properties of crystal sediments are well explored by now, the dynamics and relaxation towards equilibrium are by far less understood [10,11]. In particular, it is known

that crystallization occurs under gravity at different conditions with respect to the bulk [12,13]. The technique of colloidal templating has been used to steer colloidal crystallization layer-by-layer in gravity [14,15] and the kinetics of crystalline defects [16,17] has been debated for sediments.

Using real-space confocal microscopy techniques, Dullens and coworkers [18] have recently measured a dynamical broadening of the hard-sphere solid-fluid interface during sedimentation. This points to the essential role of crystal nucleation in the supersaturated fluid and the subsequent built-in of "crystal packages" into the interface. In a very slowly growing interface, and at low Péclet numbers, a broadening of the fluid-solid interfacial width relative to its equilibrium value was found. In this letter, we address the broadening of the solid-fluid hard-sphere interface in the sedimentation process by extensive Brownian dynamics computer simulations. We find two different types of broadenings of the fluid-crystal interface: the first occurs during growth and is correlated with the interface velocity. This type of broadening is not driven by gravity as it also shows up in the gravity-free case [19]. The second type of interface broadening occurs before the splitting of the crystal-amorphous interface from the amorphous-liquid interface. The separated interface includes a region which is structurally disordered and dynamically arrested. The latter width behaves

---

(a)E-mail: exa54@case.edu

nonmonotonously in the gravitational driving strength (or Péclet number Pe) and exhibits a huge peak relative to its equilibrium counterpart. While the first type of broadening has not yet accessed in confocal microscopy, the latter is consistent with the measurements of Dullens *et al.* [18]. However, their measurements were only performed for low Péclet numbers before the splitting of two interfaces happen.

Simulation and analysis. – In our Brownian dynamics computer simulations, we use an adapted code for hard spheres [20] of diameter σ, where the short-time infinite-dilution diffusion coefficient D_0 sets the Brownian time scale $\tau_B = \sigma^2/D_0$. A time step of $\Delta t = 0.001\tau_B$ was used in integrating the stochastic equations of motion. The simulation box contains N hard spheres and has a rectangular shape with dimensions $L_x = 40.8\sigma$, $L_y = 43.2\sigma$, and L_z varied between 54σ and 240σ. Various systems with a packing fraction $\phi = \frac{\pi\sigma^3}{6}\frac{N}{L_x L_y L_z}$ in the range $0.1 \leqslant \phi \leqslant 0.45$ were investigated. A further important system parameter is the gravitational load, or the surface (or areal) density of particles $\rho_A = N/L_x L_y$, which we scale to

$$\eta_A = N\sigma^2/L_x L_y = \phi\frac{6L_z}{\pi\sigma}. \tag{1}$$

Thus, different combinations of ϕ and L_z result in the same η_A. Simulations were carried out for $\eta_A = 45.4$ with $N = 80\,000$ particles and for $\eta_A = 90.8$ with $N = 160\,000$ particles. The quantity η_A is chosen large enough to produce a crystal-fluid interface at a given gravitational strength Pe. The gravity acceleration g points along the $-z$-direction and has a relative strength

$$Pe = mg\sigma/2k_B T, \tag{2}$$

where $k_B T$ denotes the thermal energy and m the buoyant mass of the colloidal particles. Periodic boundary conditions are employed in the x and y directions, while two hard walls are placed at $z = 0$ and $z = L_z$. Next to the wall at $z = 0$ we place a triangular layer of fixed spheres with a lattice constant $a = 1.133\sigma$ which acts as an initial template for crystal growth [21]. Without a template the crystallization happens in a few bottom layers containing small grains, large defects and fault stackings. This strongly suppresses the formation and following upward propagation of a single-phase crystalline front along the sediment.

All simulations were started from an initial configuration with a homogeneous distribution of colloids in the simulation box except the template particles in the seed layer next to the bottom wall. This mimics an initially stirred solution to which gravity is applied instantaneously [11]. A total simulation time of $500\tau_B$ was accessed during our simulations. Within this time each particle can sediment about $1000\sigma Pe$, a distance at least 5 times larger than the characteristic sedimentation length $h \approx H \times 0.55/\phi$. Here H is the hight of the sedimented
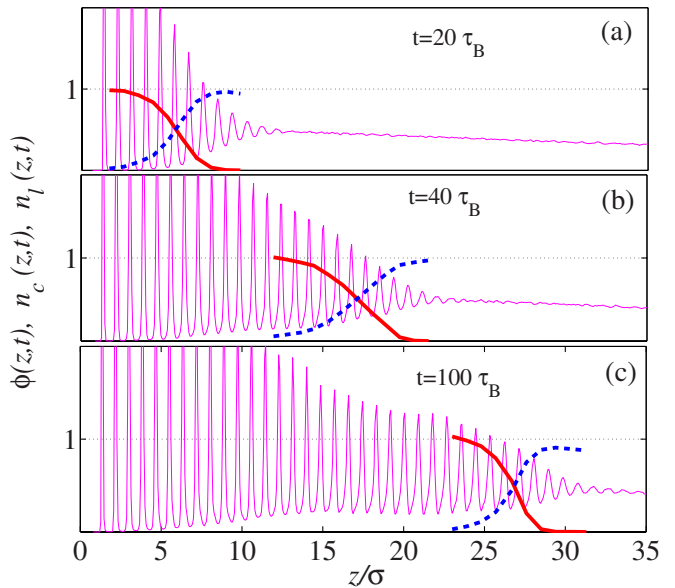

Fig. 1: (Colour on-line) Laterally averaged packing fractions $\phi(z,t)$ (thin pink lines) *vs.* reduced height z/σ for three different times (a)–(c): $t = 20\tau_B$, $40\tau_B$, $100\tau_B$. The parameters are $Pe = 0.5$, $\eta_A = 45.4$, and $\phi = 0.3$. Also shown are the interfacial profiles $n_c(z,t)$ for the "crystalline" particles (thick red line) and $n_l(z,t)$ for the "liquid-like" particles (dashed blue line). The interface position $z_0(t)$ is determined from the crossing point of the thick red and dashed blue lines.

segment above which the packing fraction of suspension is $\phi < 0.5$. We averaged our final stage and time-independent results over 20 different initial configurations in order to improve the statistics.

For subsequent times t, we calculated the laterally averaged one-particle packing fraction which is defined as

$$\phi(z,t) = \frac{\pi}{6}\frac{\sigma^3}{L_x L_y} \iint \mathrm{d}x \, \mathrm{d}y \, \rho(x,y,z,t) \tag{3}$$

and is resolved along the vertical z-coordinate. Here $\rho(x,y,z,t)$ is the local one-body density of particles at a given time t. We further identified "crystalline" particles with a crystal-like surrounding according to a commonly used criterion [22]: the local orientational-order parameter $\vec{q}_6(i)$ is calculated for each particle i [23,24]. When two particles i and j are separated by $r \leqslant 1.3\sigma$, we associate a crystalline bond to these particles, if $\vec{q}_6(i) \cdot \vec{q}_6(j) > 0.5$. A particle which has at least 8 of these bonds is considered to be crystalline. All other particles are identified as "liquid-like" particles. The corresponding local packing fractions of crystalline particles $n_c(z,t)$ and liquid particles $n_l(z,t)$ are also calculated and give rise to a q_6 interface, an example of which is given in fig. 1. We now define the *interface position* $z_0(t)$ by the implicit condition $n_c(z_0(t),t) = n_l(z_0(t),t)$, *i.e.* by the position where the fraction of crystalline-particles equals that of the liquid-like particles. The *interfacial width* $w(t)$ is defined as the
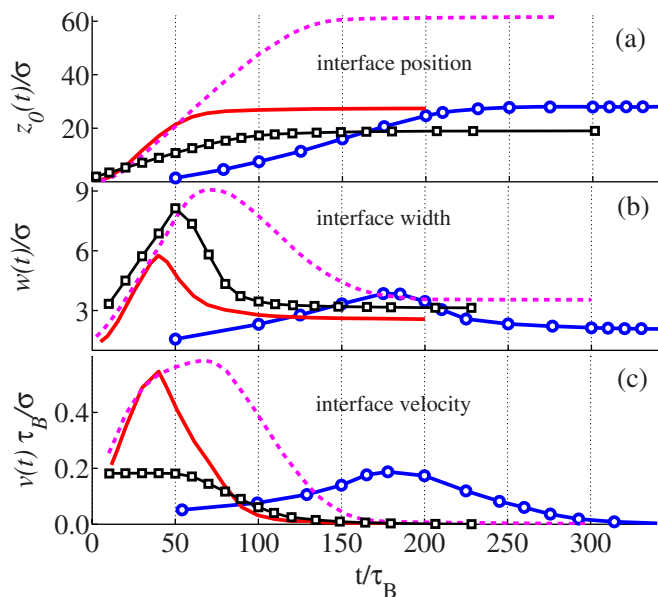
Fig. 2: (Colour on-line) Reduced interface position $z_0(t)/\sigma$ (a), reduced interfacial width $w(t)/\sigma$ (b), and reduced propagation velocity $v(t)\tau_B/\sigma$ (c) as a function of reduced time t/τ_B. The full blue lines with circles are for $\eta_A = 45.4$ and $\phi = 0.1$, the full red lines are for $\eta_A = 45.4$ and $\phi = 0.3$, the dashed pink lines are for $\eta_A = 90.8$ and $\phi = 0.3$. The full black lines with squares are simulation data for the gravity-free ($Pe = 0$) suspension with a volume fraction $\phi = 0.51$ and $\eta_A = 46.27$.

inverse of the maximal slope of the n_c profiles

$$w(t) = \left(\frac{\partial n_c(z,t)}{\partial z} \right)^{-1} \Big|_{z=z_0(t)}. \qquad (4)$$

We finally define the *propagation velocity* of the solid-fluid interface as $v(t) = \mathrm{d}z_0(t)/\mathrm{d}t$.

Mechanism 1: kinetic broadening. – Results for the interfacial profiles at three different times are shown in fig. 1. Clearly the crystal-fluid interface is propagating from the bottom of the container (left side in the figure) into the fluid. The lowering of peak heights in the density profile of fig. 1(c) in the region between $z = 14\sigma$ and $z = 27\sigma$ originates from the stacking faults [9,25] and defects introduced by a small amount of rhcp and hcp crystalline grains. These defects tend to dissipate into fcc crystalline layers during longer-time simulations. The system size also plays a crucial role in the dissipation of stacking defects [26]. When the crystal grows, the interface gets broader. This is clearly illustrated in fig. 2 where the interface position $z_0(t)$, its width $w(t)$ and its propagation velocity $v(t)$ are shown simultaneously. The interface velocity is nonmonotonic in time: it first gets accelerated, reaches a maximum and decays to zero. The initial acceleration has to do with an "induction time" to get particles into positions which are structurally favorable for subsequent crystal growth. The final slowing-down is due to the approach to equilibrium where ideally a finite

height of the interface is reached. Concomitantly with the nonmonotonic behavior of the interface velocity, there is a broadening of the interface: as a function of time, it first broadens and then shrinks again. The saturation value at large times, however, is significantly larger than the initial width. A direct comparison of figs. 2(b) and (c) reveals that the maximum of the propagation velocity coincides with the maximal interfacial width demonstrating that these two phenomena are correlated. The effect is stable for different overall densities η_A. An increased η_A just retards the occurrence of the velocity and width maximum such that they occur at larger simulation times. A similar retardation effect takes place in systems with low packing fraction ϕ at a fixed areal density η_A, compare solid lines with and without symbols in fig. 2.

As a first type of interfacial widening, we therefore identify a *kinetic broadening* of the interface: upon growth, the q_6-interface becomes less steep, see thick lines in fig. 1(b). This has to do with the fact that the system has less time to structurally arrange when the interface propagates quickly. An additional simulation for zero gravity revealed that the kinetic broadening effect exists also at zero Péclet number[1]. However, in the gravity-free case the front growth velocity has no maximum. As a reference, simulation data for the front position, interfacial width and the propagation velocity for a coexisting fluid and crystal [22,27,28] in a gravity-free system are included into fig. 2 as full lines with squares.

Mechanism 2: interface splitting. – We now address the crystal-fluid interface in the final state of the sediment after a long time $t_l = 500\tau_B$ and discuss its properties as a function of the Péclet number (at fixed η_A). In fig. 3, the laterally averaged packing fraction profiles are shown at t_l for three different Péclet numbers, $Pe = 0.5, 1.6, 3.0$. Interestingly, the position of the interface (as visualized by the crossing of the red and blue lines) behaves nonmonotonously in the Péclet number, see also fig. 4, which contradicts the expectation based on equilibrium arguments. This expectation is based on a discussion of the two limiting cases $Pe \to 0$ and $Pe \to \infty$ in equilibrium: for zero gravity, the density profile is homogeneously distributed over the full simulation box (apart from local density correlations at the hard wall) with a low bulk volume fraction. Hence the solid-fluid interface (if at all) is close to the bottom wall. In the opposite limit $Pe \to \infty$, there is a finite number of layers with a closed packed density which then abruptly drops to a vacuum at higher Pe at a height of about 30σ. Interpolating between these two limiting cases, in equilibrium, the interface position increases with Péclet number Pe. Starting from $Pe \approx 0.8$ the single crystalline-liquid interface splits

---

[1]The $Pe = 0$ simulation was performed for $\phi = 0.51$ and $\eta_A = 46.27$ with $N = 80\,000$ particles in a box of size $L_x = 40.8\sigma$, $L_y = 43.2\sigma$, and $L_z = 48.5\sigma$. Again a template layer of fixed spheres with a triangular layer lattice constant $a = 1.133\sigma$ was placed above the bottom plate of the box.
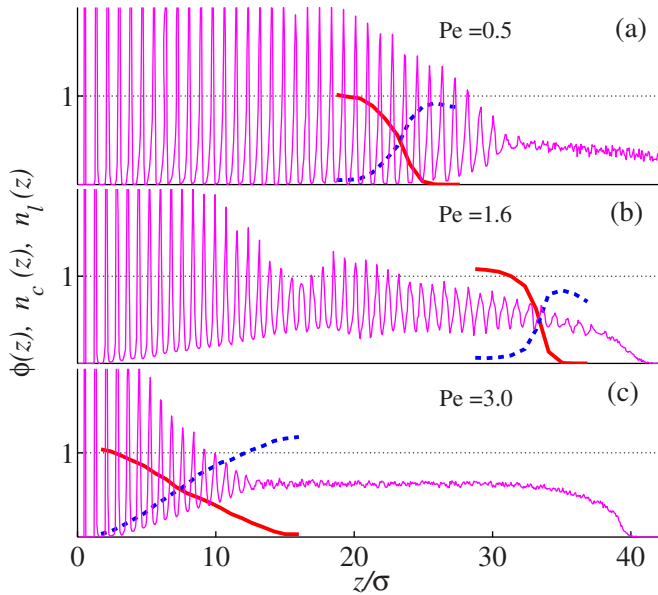
Fig. 3: (Colour on-line) Same as fig. 1, but now for a fixed large time $t = t_l = 500\tau_B$ and three different Péclet numbers: (a) $Pe = 0.5$, (b) $Pe = 1.6$, (c) $Pe = 3.0$ at $\eta_A = 45.4$ and $\phi = 0.1$.

into two separate interfaces, the crystalline-amorphous and the amorphous-liquid interfaces. When the gravitational load increases, the amount of amorphous glass grows partly from the sedimented liquid particles, and partly from the collapsed crystalline layers. Higher loads completely destroy the crystal leaving only a few intact layers. Besides the q_6-interface position, a position of the amorphous-liquid interface can be defined at the height where the coarse-grained density (averaged over the oscillations)[2] equals the bulk coexisting fluid volume fraction of 0.492. As opposed to the nonmonotonic variation of the q_6-interface position, the position of the amorphous-liquid interface is monotonic, see fig. 4. While the positions of the q_6-interface and the amorphous-liquid interface coincide for small Péclet number, there is a *splitting* above a threshold leading to the nonmonotonic behavior. The nonmonotonicity can be explained by the formation of a dynamically arrested region between the splitted q_6 and amorphous-liquid interfaces schematically shown in fig. 5(a) for a system with $\phi = 0.3$, $\eta_A = 90.8$ and $Pe = 2$. Within the glassy amorphous region the particles are structurally disordered, see fig. 5(b), and dynamically caged such that they cannot find suitable surrounding to nucleate into a big, and layered, crystal. This is documented by the smallness of the mean square displacement of particles in the amorphous layer, see fig. 5(c). The amorphous dynamically arrested part stops the propagation of the q_6-interface. Strong gravity acts therefore like a fast and deep compression, a situation which favours glass formation in general. The disordered

---

[2]In detail, the coarse-grained density is obtained from the z-resolved profiles by integrating between two subsequent minima.
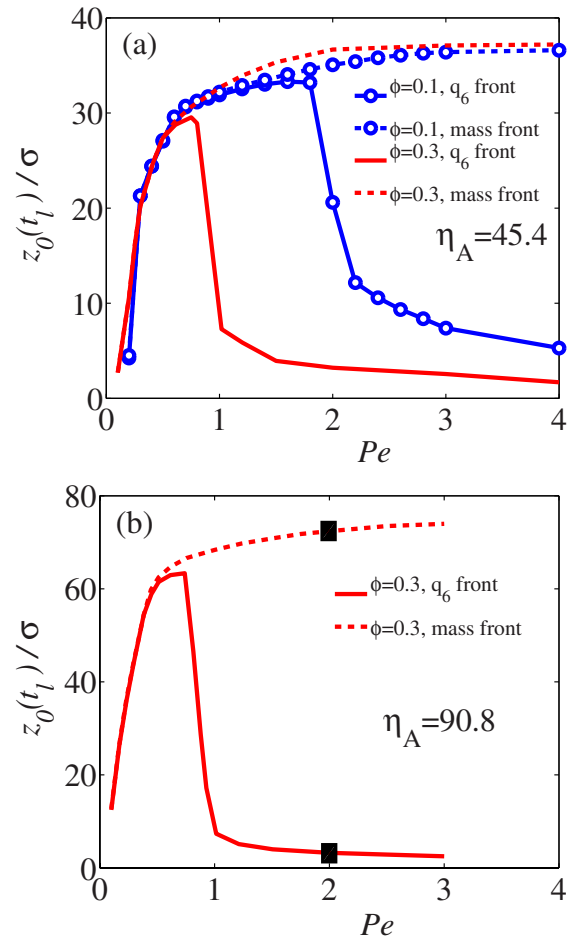

Fig. 4: (Colour on-line) (a) Position $z_0(t_l)/\sigma$ of the q_6-interface (full lines), and of the amorphous-liquid interface (dashed lines) *vs.* Péclet number Pe for two areal densities $\eta_A = 45.4$ (a) and $\eta_A = 90.8$ (b) at a fixed large time $t = t_l = 500\tau_B$. The interface splitting is clearly visible. The black squares at $Pe = 2$ correspond to the amorphous-liquid and q_6-interfaces analyzed in fig. 5.

region does not seem to be composed of polycrystalline material as this would have resulted in a finite fraction of crystalline particles. As shown in figs. 4(a) and (b), the Péclet number threshold for splitting decreases for increasing packing fraction ϕ at fixed η_A, but does not depend on the imposed overall density η_A for fixed ϕ. Closely above the Péclet number threshold at which interface splitting occurs, the width w exhibits a strong peak, see fig. 6. In fact, the width increases by an order of magnitude relative to its low-Péclet-number value and then decreases again. This surprising huge broadening points to an extremely broad interface between the initial crystalline layers and the subsequently formed disordered material. The subsequent decrease for higher Péclet number is qualitatively understood by considering the limit $Pe \to \infty$: if everything is dominated by strong gravity, the interface then is expected to sharpen due to enforced crystallization.
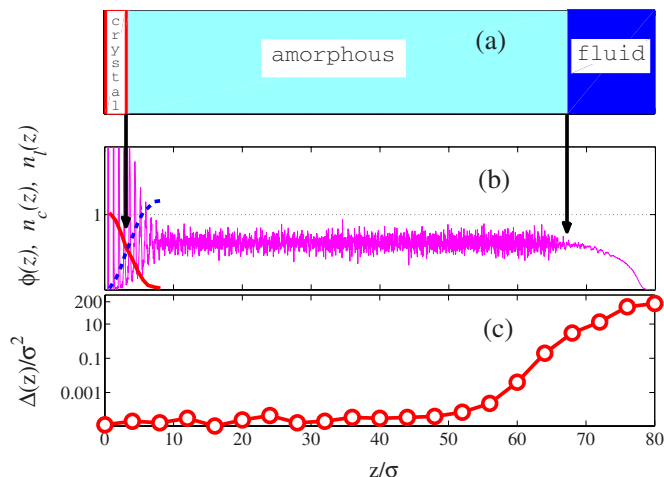
Fig. 5: (Colour on-line) Simulation results for the sediment at $t = t_l = 500\tau_B$ for system parameters $Pe = 2$, $\phi = 0.3$ and $\eta_A = 90.8$. (a) Schematic picture showing the crystalline, amorphous and fluid zones in the sediment. (b) Laterally averaged packing fraction $\phi(z)$ (thin pink lines), interfacial profile $n_c(z)$ for the "crystalline" particles (thick red line), interfacial profile $n_l(z)$ for the "liquid-like" particles (dashed blue line) vs. reduced height z/σ. (c) Mean square displacement $\Delta(z)$ of the particles along the sediment obtained within a time window $\Delta t = 10\tau_B$. The positions of the crystal-glass and glass-fluid interfaces correspond to the black squares in fig. 4(b).

Fig. 6: (Colour on-line) Interfacial width $w(t_l)/\sigma$ vs. Péclet number Pe at a fixed large time $t = t_l = 500\tau_B$ for two different packing fractions $\phi = 0.1$ (line with symbols) and $\phi = 0.3$ (full line) at fixed areal density $\eta_A = 45.4$, and for packing fraction $\phi = 0.3$ and $\eta_A = 90.8$ (dashed line).

We now compare our results to the real-space experiment by Dullens and coworkers [18]. The broadening observed in ref. [18] was measured for long times at relatively small Péclet numbers (smaller than 0.8) and for larger gravitational loads η_A than considered in our work. The interfacial velocity was small but nonzero. This implies that the broadening observed in [18] is consistent with our findings at long times for low Pe, before the interface splitting occurs. It would be interesting to do further experiments at higher Pe to verify the interface splitting and the huge interface broadening predicted by our simulations.

Conclusion. – In conclusion, we have studied the width of a crystal-fluid interface in a sedimenting suspension of hard spheres by Brownian dynamics computer simulations. Two qualitatively different types of broadening are observed. The first type of interfacial broadening is purely kinetic. It is not triggered by gravity but just correlates with the interface velocity. The second type of broadening is almost static and is huge if the structural crystallinity interface and the amorphous-liquid interface split. Between these two interfaces, an amorphous dense sediment is formed which exhibits a wide structural interface with the lower crystalline part of the sample. This prediction can in principle be verified by real-space experiments [18,22]. It might also be important for granulates [29] where the Péclet number is high, and for crystallization in complex plasma [30].
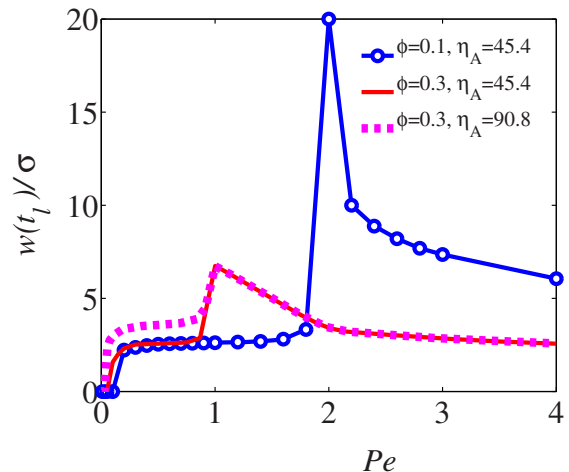
Real experimental samples possess an intrinsic polydispersity. Furthermore there are solvent-mediated hydrodynamic interactions. Most of the influence of hydrodynamic interactions can be captured by an effective short-time diffusion constant D_0. Nevertheless the influence of polydispersity [22] and hydrodynamic interactions [11,31,32] on crystal growth remains for future exploration. Furthermore new effects are expected for attractive systems [33] as witnessed by different dynamically arrested states (attractive glasses) [34] which could impede crystallization during sedimentation. The latter case is realized for colloid-polymer mixtures.

It is worth mentioning that some of the present findings on the interface broadenings may be characteristics of fcc {111} growth from a patterned template with the triangular lattice considered in the current study. It will be useful to check whether a similar broadening takes place in the {100} growth, a case considered in refs. [27,28] for gravitation-free hard-sphere systems.

In general, our findings can be used to steer the thickness of crystalline and amorphous layers as well as their interfacial structure by sedimentation. This may help to open the way for designing smart colloidal materials with new optical and rheological properties.

$* * *$

REFERENCES

[1] Naudin J. J., Cauwet G., Chretiennot-Dinet M. J., Deniaux B., Devenon J. L. and Pauc H., *Estuar. Coast. Shelf Sci.*, **45** (1997) 303.

[2] Walter H. and Albertsson P. A., *Exp. Cell Res.*, **67** (1971) 218.

[3] Philipse A. P., *Curr. Opin. Colloid Interface Sci.*, **2** (1997) 200.

[4] Piazza R., Bellini T. and Degiorgio V., *Phys. Rev. Lett.*, **71** (1993) 4267.

[5] Biben T., Hansen J. P. and Barrat J. L., *J. Chem. Phys.*, **98** (1993) 7330.

[6] Davidchack R. L. and Laird B. B., *J. Chem. Phys.*, **108** (1998) 9452.

[7] Biben T., Ohnesorge R. and Löwen H., *Europhys. Lett.*, **28** (1994) 665.

[8] Marechal M. and Dijkstra M., *Phys. Rev. E*, **75** (2007) 061404.

[9] Mori A., Yanagiya S., Suzuki Y., Sawada T. and Ito K., *J. Chem. Phys.*, **124** (2006) 174507.

[10] Royall C. P., Dzubiella J., Schmidt M. and van Blaaderen A., *Phys. Rev. Lett.*, **98** (2007) 188304.

[11] Wysocki A., Royall C. P., Winkler R., Gompper G., Tanaka H., van Blaaderen A. and Löwen H., *Soft Matter*, **5** (2009) 1340.

[12] Ackerson B. J., Paulin S. E., Johnson B., van Megen W. and Underwood S., *Phys. Rev. E*, **59** (1999) 6903.

[13] Cheng Z. D., Chaikin P. M., Zhu J. X., Russel W. B. and Meyer W. V., *Phys. Rev. Lett.*, **88** (2002) 015501.

[14] Hoogenboom J. P., Derks D., Vergeer P. and van Blaaderen A., *J. Chem. Phys.*, **117** (2002) 11320.

[15] Ramsteiner I. B., Jensen K. E., Weitz D. A. and Spaepen F., *Phys. Rev. E*, **79** (2009) 011403.

[16] Mori A., Suzuki Y. and Yanagiya S. I., *Fluid Phase Equilib.*, **257** (2007) 131.

[17] Hoogenboom J. P., Vergeer P. and van Blaaderen A., *J. Chem. Phys.*, **119** (2003) 3371.

[18] Dullens R. P. A., Aarts D. G. A. L. and Kegel W. K., *Phys. Rev. Lett.*, **97** (2006) 228301.

[19] This finding contrasts the simple Ginzburg-Landau theory for the interfacial dynamics of a one-component non-conserved order parameter profile (like the crystallinity). Under the assumption that the curvatures of the free energies in order parameter space are independent of the undercooling, the interfacial width *shrinks* with its propagation velocity, see *e.g.*: Bechhoefer J., Löwen H. and Tuckerman L. S., *Phys. Rev. Lett.*, **67** (1991) 1266.

[20] Cichocki B. and Hinsen K., *Physica A*, **166** (1990) 473.

[21] Heni M. and Löwen H., *Phys. Rev. Lett.*, **85** (2000) 3668.

[22] Sandomirski K., Allahyarov E., Löwen H. and Egelhaaf S. U., to be published in *Soft Matter* (2011) DOI: 10.1039/c1sm05346a.

[23] Steinhardt P. J., Nelson D. R. and Ronchetti M., *Phys. Rev. B*, **28** (1983) 784.

[24] ten Wolde P. R., Ruiz-Montero M. J. and Frenkel D., *Phys. Rev. Lett.*, **75** (1995) 2714.

[25] Mori A., Suzuki Y., Yanagiya S. I., Sawada T. and Ito K., *Mol. Phys.*, **105** (2006) 1377.

[26] Mori A., *J. Cryst. Growth.*, **318** (2011) 66.

[27] Zykova-Timan T., Horbach J. and Binder K., *J. Chem. Phys.*, **133** (2010) 014705.

[28] Mori A., *J. Phys. Soc. Jpn.*, **66** (1997) 1579.

[29] Both J. A. and Hong D. C., *Phys. Rev. E*, **64** (2001) 061105.

[30] Rubin-Zuzic M., Morfill G. E., Ivlev A. V., Pompl R., Klumov B. A., Bunk W., Thomas H. M., Rothermel H., Havnes O. and Fouquét A., *Nat. Phys.*, **2** (2006) 181.

[31] Nguyen N. Q. and Ladd A. J. C., *J. Fluid Mech.*, **525** (2005) 73.

[32] Moncho-Jorda A., Louis A. A. and Padding J. T., *Phys. Rev. Lett.*, **104** (2010) 068301.

[33] Leocmach M., Royall C. P. and Tanaka H., *EPL*, **89** (2010) 38006.

[34] Zaccarelli E., Löwen H., Wessels P. P. F., Sciortino F., Tartaglia P. and Likos C. N., *Phys. Rev. Lett.*, **92** (2004) 225703.